Biosensors and Bioelectronics 130 (2019) 236–244

Contents lists available at ScienceDirect

Biosensors and Bioelectronics

journal homepage: www.elsevier.com/locate/bios

Design of peptide nucleic acid probes on plasmonic gold nanorods for detection of circulating tumor DNA point mutations

Amogha Tadimety[a], Yichen Zhang[a], Kasia M. Kready[a], Timothy J. Palinski[a], Gregory J. Tsongalis[b,c], John X.J. Zhang[a,c,*]

[a] Thayer School of Engineering, Dartmouth College, 14 Engineering Drive, Hanover, NH 03755, USA
[b] Laboratory of Clinical Genomics and Advanced Technology, Department of Pathology and laboratory Medicine, Dartmouth Hitchcock Medical Center, Lebanon, NH 03766, USA
[c] Norris Cotton Cancer Center, Dartmouth Hitchcock Medical Center, Lebanon, NH 03766, USA

ARTICLE INFO

Keywords:
Localized surface plasmon resonance (LSPR)
Liquid biopsy
Nanosensor
Circulating tumor DNA
Point mutation
Nanorods
Surface conjugation

ABSTRACT

Here we present a gold nanorod-based platform for the sequence-specific detection of circulating tumor DNA (ctDNA) point mutations without the need for amplification or fluorescence labeling. Peptide nucleic acid probes complimentary to the G12V mutation in the KRAS gene were conjugated to gold nanorods, and the localized surface plasmon resonance absorbance through the sample was measured after exposure to synthetic ctDNA at various concentrations. Each step of the reaction was thoroughly controlled, starting from reagent concentrations and including conjugation, sonication, and incubation time. The platform was evaluated in both buffer and spiked healthy patient serum, demonstrating a linear working range below 125 nanograms of ctDNA per milliliter solution, and an effective limit of detection of 2 nanograms of ctDNA per milliliter. A clear distinction between mutant and wild type synthetic ctDNA was also found using this platform. In order to improve upon the selectivity of the sensor, a DNA hybridization simulation was performed to understand how the addition of mutations to the peptide nucleic acid probe could enhance the selectivity for capture of mutant over wild type sequences. The top candidate from the simulations, which had an additional mutation two base pairs away from the mutation of interest, had a significant impact on the selectivity between mutant and wild type capture. This paper provides a framework for sequence-specific capture of ctDNA, and a method of improving selectivity for desired point mutations through careful probe design.

1. Introduction

Cancer is a leading cause of death in the United States and worldwide, with more than 1.5 million new cases and 600 thousand deaths in the US alone projected in 2018 (Siegel et al., 2018). While much of cancer research focuses on developing new therapies and imaging modalities, there is general agreement among healthcare providers that earlier diagnosis and better monitoring of cancer could reduce the number of cancer mortalities each year. Current cancer diagnosis takes into account a combination of patient symptoms, imaging, and tissue biopsy, but can be costly, invasive, and time-intensive for the patient (Tadimety et al., 2017b). Liquid biopsy is a promising technique that harnesses biomarkers circulating in a biofluid, rather than in a tissue sample, to characterize the tumor (Hao and Zhang, 2017; Tadimety et al., 2018; Tadimety et al., 2017a). This process could have a number of advantages relative to the conventional clinical workflow, including minimal invasiveness for the patient, quicker time-to-result, and the ability to screen without knowing the primary tumor type.

Liquid biopsy looks at a range of biomarkers including circulating tumor cells, exosomes, circulating nucleic acids, and proteins (Anker et al., 1999; Egatz-Gomez et al., 2016; Jia et al., 2015; Zhang et al., 2017). All are shed off of the tumor into the bloodstream and peripheral body fluids, and there are a number of technologies looking to capture and analyze these biomarkers (Chen et al., 2015; Hoshino et al., 2015; Joshi et al., 2015; Ozkumur et al., 2013). Circulating tumor DNA (ctDNA) is one such biomarker that is thought to be clinically relevant because it can inform about both the genetic and epigenetic changes taking place in the tumor at a single time point, as it has a very short half-life in peripheral blood (Bettegowda et al., 2014; Jiang and Lo, 2016). One mutation hotspot that is commonly studied is exon 2 of the KRAS gene, a gene that is implicated in a number of cancers including pancreatic ductal adenocarcinoma, which is associated with extremely

* Corresponding author at: Thayer School of Engineering, Dartmouth College, 14 Engineering Drive, Hanover, NH 03755, USA.
E-mail address: john.zhang@dartmouth.edu (J.X.J. Zhang).

https://doi.org/10.1016/j.bios.2019.01.045
Received 30 October 2018; Received in revised form 6 January 2019; Accepted 19 January 2019
Available online 29 January 2019
0956-5663/

poor prognosis (López et al., 2016; Tadimety et al., 2017b).

Due to the low concentration of ctDNA and relatively low percentage of mutant ctDNA, both the sensitivity and specificity of the sensor are critically important. The most common current methods of ctDNA detection include the use of digital polymerase chain reaction (PCR), droplet digital PCR, or next generation sequencing to detect and quantify circulating tumor DNA and clinically relevant mutations (Dawson et al., 2013; Kinugasa et al., 2015; López et al., 2016; Sausen et al., 2015). These methods require amplification and thus have a time-to-result in the range of hours, and can be cost prohibitive, requiring expensive equipment and technician time.

One promising strategy that can be used to develop a high sensitivity sensor is plasmonics, an optical phenomenon arising from the interface between metal and dielectric (Guo and Kim, 2012; Lin et al., 2016; Sepúlveda et al., 2009). Gold nanoparticles exhibit a number of plasmonic phenomena, including localized surface plasmon resonance (LSPR), Rayleigh scattering, the scattering of light by particles, and Raman spectroscopy, the scattering of molecules as they adsorb onto nanostructured surfaces (Braun et al., 2007; Im et al., 2013; Ngernpimai et al., 2018). LSPR in particular presents a straightforward and direct label-free method of detecting specific ctDNA sequences. These properties offer further benefits over other mentioned plasmonic systems including enhanced field confinement, higher sensitivity, and ease of use (Brolo, 2012).

The highly confined electric fields of the LSPR modes on the nanoparticles serve as a sensitive transducer to changes in the local dielectric environment of the nanoparticle. Because of the relationship between the resonance of the particle and the local refractive index, LSPR sensors have been shown to demonstrate increasing wavelength spectral resonant shifts to monolayers of increasing size (Mayer and Hafner, 2011). The Drude model shows that the peak LSPR energy decreases with increasing refractive index, and red shifted plasmon resonances are lower energy: this is consistent with layers binding to the nanoparticle causing red shift in the plasmon resonance (Mayer and Hafner, 2011). To apply this principle to a selective biosensor, the sensor is appropriately functionalized to selectively capture the biomarker of interest, and the nanoparticles will exhibit successive red-shifts in the optical response with increasing biomarker concentration (Joshi et al., 2015; Ma et al., 2015; Nguyen and Sim, 2015). Single molecule detection has been demonstrated using the LSPR principle (Taylor and Zijlstra, 2017).

In this paper, we propose a gold nanorod-based plasmonic detection workflow including a description of conjugation and sensing protocols, and demonstration of a novel capture probe design process. As shown in Fig. 1, the platform uses a peptide nucleic acid (PNA) probe that is specific to the point mutation of interest conjugated to gold nanorods. The results walk through an iteration of existing standard EDC-NHS cross-linking protocols to determine the ideal concentration and incubation times. Then selective biosensing is demonstrated, along with a strategy to improve the selectivity for the mutant allele over the wild-type through hybridization simulations. Ultimately, this paper provides a framework for the design of highly sensitive and selective sensors for quantitation of ctDNA from a serum sample and calculation of mutant allele fractions.

2. Material and methods

2.1. Reagents and buffers

Carboxylated gold nanorods with dimensions 40 nm × 124 nm and a longitudinal resonance peak at 780 nm were used (Nanopartz Inc). Baseline absorbance in TE buffer (10 mM Tris-HCl and 0.1 mM EDTA, ThermoFisher) and 10 mM CTAB surfactant were measured prior to starting conjugation to acquire the starting absorbance spectrum. All absorbance measurements were taken of 2uL sample on the Tecan NanoQuant Plate using the Tecan Spark 10 M Microplate Reader with a wavelength range between 400 nm and 1000 nm and a step size of 1 nm. 15 bp HPLC-purified PNA probes functionalized with a free amine group were purchased (PNABio) with the G12V KRAS mutation centered and were stored diluted to 100 µM in molecular grade water. An activation buffer was made in-house using molecular grade water, 0.1 M MES and 0.5 M NaCl and buffered to pH 6.0 (ThermoFisher). 41 bp synthetic ctDNA oligonucleotides were purchased from Integrated DNA Technologies (IDT) and were suspended and stored in sterile TE buffer to a final concentration of 100 µM. The sequences of each of these probes is listed in the Supplementary Information.

2.2. PNA conjugation onto gold nanorods

The nanorod conjugation protocol was modified from a number of sources describing standard EDC-NHS crosslinking chemistry (Jazayeri et al., 2016; Lohse et al., 1999; Ray and Nordén, 2000; Wang et al., 2003; Wang and Sim, 2006; Zhang and Appella, 2010). The pH was carefully controlled through the process so that the EDC-NHS coupling occurred at pH of 6.0, but the PNA conjugation occurred at physiological pH of 7.0. This was done through the use of an activation buffer at pH of 6.0 and the addition of a carbonate-bicarbonate buffer to bring the pH to 7.0 for the PNA coupling. The ctDNA binding occurred in serum or Tris-EDTA (TE) buffer at a pH close to 7.5, as described in Section 2.4.

375 mM stock of 1-Ethyl-3-(3-dimethylaminopropyl)-carbodiimide (EDC) and 937.5 mM N-hydroxysuccinimide (NHS) stock were prepared in molecular grade water (Sigma Aldrich). 20 µL of carboxylated 40 nm rods with a baseline absorbance at 780 nm were placed into a low

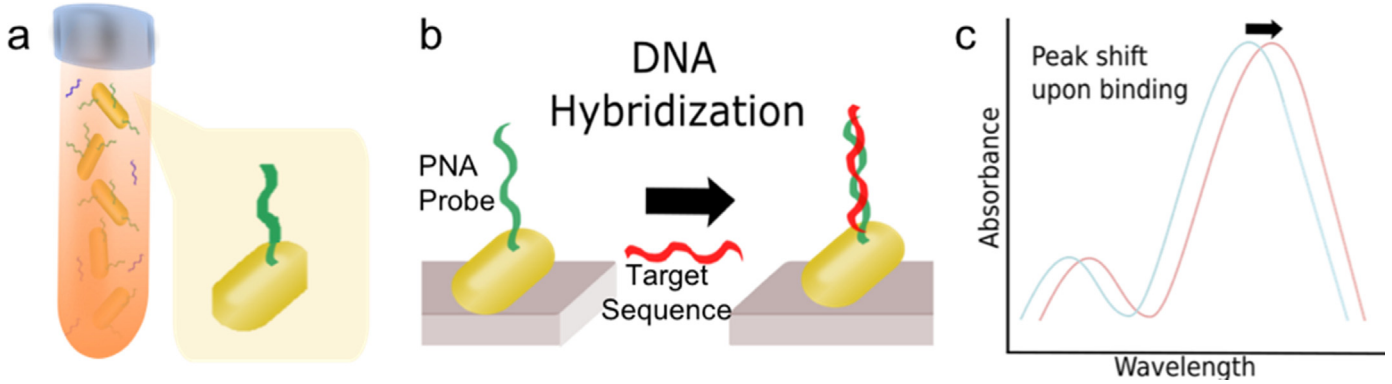

Fig. 1. (a) Gold nanorods in patient fluid sample with probe complimentary to ctDNA of interest. (b) ctDNA hybridization onto PNA on gold nanorod. (c) Resonant red shift in the absorbance through the sample upon ctDNA binding to the PNA probe at the gold nanorod surface, with the blue curve representing the resonance before binding, and the red curve after.

retention Eppendorf tube (Fisher Scientific) and centrifuged at 6000 rpm for 8 min to separate the particles from the solution. The supernatant was removed and 100 µL of 10 mM cetyltrimethylammonium bromide (CTAB) was added to redisperse the rods. The rods were then sonicated in ice cold water, and the starting spectrum was measured before the rods were centrifuged once again. Once the rods had pelleted, 1 µL each of the EDC and NHS solutions were added along with 98 µL of activation buffer and incubated together for 15 min while mixing. After this activation step, the nanorods were centrifuged once again to remove excess NHS in the supernatant before addition of 2.4 µL of the peptide nucleic acid (PNA) and 97.6 µL of Activation buffer raised to a pH of 7.0 (using carbonate-bicarbonate buffer). The reaction tube was sonicated in ice cold water until nanorods were resuspended, and the reaction was allowed to proceed for two hours at room temperature. After incubation, the resulting rods were resuspended using sonication and absorbance was measured to verify successful conjugation before storing in the fridge for up to a week.

2.3. PNA hybridization simulations

Peptide nucleic acids (PNAs) were used for sequence-specific capture of ctDNA in solution due to their stability and specificity to the sequence of our molecule of interest. PNAs are a structural hybrid between a protein and a nucleic acid, with the backbone of a protein and functional nitrogenous bases linked through a tertiary acetamide (Siddiquee et al., 2015). Importantly, PNAs have been shown to demonstrate stronger binding regardless of the salt concentration in solution, and have better strand invasion of duplex DNA targets to form PNA/DNA duplexes (Siddiquee et al., 2015). The two-state hybridization application on DINAMelt, an open resource from the Rensselaer Polytechnic Institute, was used to determine the binding affinity of the probes to the DNA sequence of interest under physiological conditions. A room temperature of 25 °C was used, with a salt ion concentration of 0.14 M and a concentration of strands comparable to those used in testing. A range of mutations including the central mutation at c.35G > T were used with increasing distance from the mutation of interest. The application returned the calculated melting temperatures for the probe-ctDNA duplexes for the 41 bp wild type and mutant sequences, demonstrating the binding affinity for the duplexes.

2.4. Synthetic ctDNA capture in buffer and spiked healthy patient serum

ctDNA sensing was demonstrated by incubating conjugated gold nanorods with known quantities of synthetic ctDNA oligos in either TE buffer or healthy patient serum. A final gold nanorod concentration of OD 0.25 was used, which corresponds to a 4.67×10^9 nanorods/mL, or about 7.75 pM. The incubation period lasted for 10 min. After incubation, the gold nanorods were sonicated in ice cold water for 20 s before the absorbance measurement was taken.

All capture measurements were benchmarked using the Qubit 2.0 fluorometer with the Qubit DNA Assay Kit. These experiments were used to calculate the percentage of starting ctDNA bound to the sensor to validate the sensor. After the gold nanorods were put in contact with the synthetic ctDNA oligos for the incubation period, the sample was centrifuged, and the supernatant collected to quantify the remaining oligo. The samples were diluted to a working volume of 200 µL and compared to a small sample of the starting solution to calculate the amount of starting oligo that had bound to the nanorod sensors.

3. Results and discussion

3.1. Principle of the sensor and workflow

The whole process demonstrated in this paper takes place in solution, including conjugation, ctDNA binding, and absorbance measurement after binding. To create a nanoplasmonic sensor starting from gold nanorods, the first step was to choose a target and optimize the surface conjugation protocol for ideal sensing. Once the starting nanorod was acquired, a series of experiments were run to determine the ideal concentrations and incubation times for maximum surface conjugation efficiency of PNAs onto the gold nanorod.

After the conjugation protocol was optimized, a range of nanorod concentrations in solution were tested to determine the optimal concentration for ctDNA sensing. The transduction mechanism of the rods has to do with the electromagnetic wave oscillations at the metal-dielectric interface. Any binding to the rod changes this oscillation leading to a change in the peak absorbance wavelength of the nanorod. To measure this, the nanorods were suspended into solutions with known concentrations of ctDNA to measure their binding capabilities in both TE buffer and in spiked serum samples, and the performance of the sensor was tested. Finally, some work was done to optimize selectivity through addition of secondary mutations into the PNA sequence to increase the difference in binding affinity to both the mutant and wild type target sequences, and this technique was demonstrated both in simulation and experimentally.

3.2. PNA probe selection for pancreatic ductal adenocarcinoma

Because ctDNA is DNA derived directly from the tumor, it provides a snapshot of the somatic mutations in the tumor in real time (Bettegowda et al., 2014). For this proof-of-concept we chose to develop the sensor for pancreatic ductal adenocarcinoma due to its significant death rate, which is partially thought to be caused by a lack of clinically relevant biomarkers and sensitive diagnostics for early detection of disease. For a ctDNA target relevant to pancreatic cancer, the KRAS mutation was an obvious choice with a prevalence rate of 88% in pancreatic cancers, and the most common mutations are found in coding base 35 of exon 2 (Kinugasa et al., 2015; Sausen et al., 2015). We chose the c.35G > T mutation, which replaces glycine 12 with a valine (G12V) residue. This particular mutation has a prevalence of 37% in pancreatic cancers, and was the most common mutation in the KRAS gene from a 2015 clinical study done by Sausen et al. (2015) and Kinugasa et al. (2015).

To demonstrate the applicability of this platform, we wanted to be able to quantify the concentration of this mutation and the background wild type KRAS in a sample at a clinically relevant level. As described earlier, we chose to use a peptide nucleic acid (PNA) probe complimentary to this particular sequence and attached it to the gold nanorods through cross linking chemistry. Both the process required for PNA conjugation to nanorods and the location of the G12V mutation within the gene are shown in Fig. 2. We also conducted a PNA-DNA binding simulation to determine the thermodynamic constants of this binding reaction, as described in the methods. From this simulation, we determined that the melting temperature of the G12V PNA to synthetic ctDNA of the relevant sequence would have a melting temperature of 47.2 °C compared to 42.5 °C for its binding to the wild type sequence.

3.3. Conjugation optimization

The protocol for conjugation was modified from a number of existing papers describing the EDC-NHS crosslinking chemistry (Jazayeri et al., 2016; Lohse et al., 1999; Ray and Nordén, 2000; Wang et al., 2003; Wang and Sim, 2006; Zhang and Appella, 2010). Because of the LSPR effects, we expect red shifts (shifts towards the right, longer wavelengths) with molecule binding to the surface of the rods, as described in the Introduction. In the process of the conjugation, we were able to benchmark whether the conjugation was working through repeated measurements of the absorbance of the gold nanorods.

As seen in Fig. 3**a**, the removal of the surfactant CTAB and activation with NHS leads to a slight blue shift in the peak (towards the left) because the activated NHS molecule is slightly smaller than CTAB

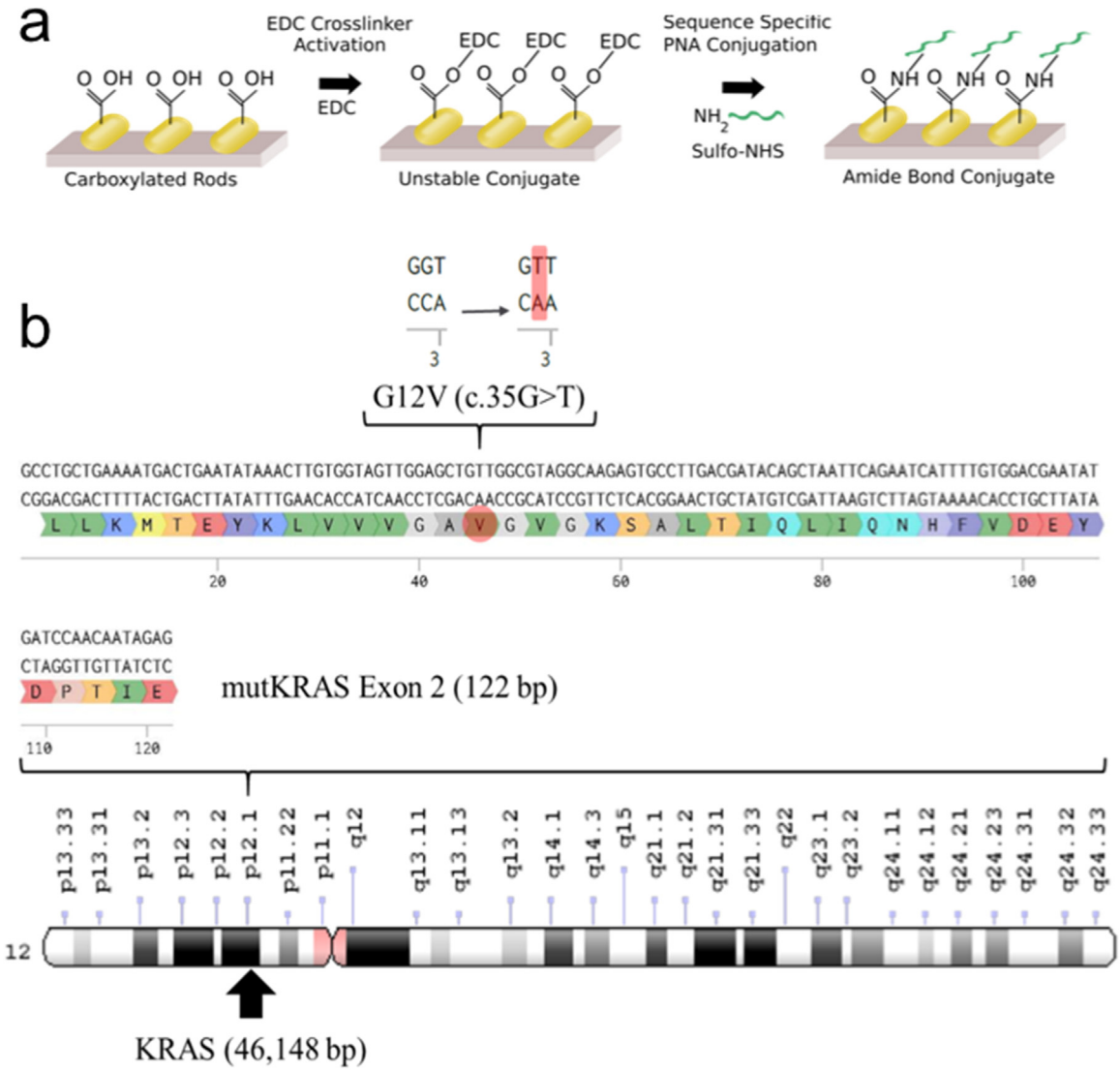

Fig. 2. (a) A demonstration of conjugation workflow from bare gold nanorods to PNA conjugation using EDC-NHS coupling (b) A schematic demonstrating the location of the G12V mutation within Exon 2 of the KRAS gene. Schematic was created using Benchling.

surfactant. Then, after the PNA conjugation, the absorbance peak shifts significantly towards the red with a peak around 900 nm and flattens. This may be explained by the gel-like quality of the PNA probes causing the nanorods to coagulate into larger clumps, which characteristically have a peak at higher wavelengths. TEM images of this clumping of nanorods can be found in the Supplementary Information, and similar phenomena have been reported in the literature (Kedem et al., 2011). After contact with the ctDNA oligos the peak shifts back towards about 800 nm as the nanorods successfully disperse again. This significant red shift and flattening became the expected outcome of a successful conjugation and was used in further experiments to determine the conjugation success rate.

Next, we tested the correct incubation time to determine how long the gold nanorods needed to be in contact with the ctDNA to give us the best output. A nanorod concentration of 0.5 OD was used with a synthetic ctDNA concentration of 50 ng/mL as a starting point for these experiments. A clear red shift is seen after approximately 10 min of incubation, indicating that 10 min is the minimum amount of time for the ctDNA to bind to the nanorods and transduce a measurable signal, and that 10 min may be optimal (Fig. 3**b**). The large variance in the data can be described by the clumping behavior of the nanorods and is corrected for in later experiments.

Next, we studied the optimal concentration of gold nanorods to use for sensing, as shown in Fig. 3**c**. There is a trade off with the concentration of nanorods, because the absorbance peak is easier to see with a higher concentration of gold nanorods, but more nanorods means more binding sites for ctDNA and therefore a lower sensitivity. We only tested fairly low concentrations of the gold nanorods in the final solution and looked into the percent of starting ctDNA that bound to the sensor at a range of concentrations less than OD 0.5. The nanorods were put in contact with the ctDNA in solution and after incubation were measured and then centrifuged so that the supernatant could be collected for ctDNA binding quantitation. From this study we determined that, as expected, the amount of ctDNA bound on the nanorods decreases with decreasing nanorod concentration, as there are fewer binding sites. From this study, a nanorod concentration of OD 0.25 was used for further experiments.

One last experimental parameter that was investigated was the amount of time that the nanorods were sonicated for dispersal during testing and after conjugation. We found, as shown in Fig. 3**d**, that after approximately 30 s of sonication, there was a blue shift of the nanorod absorbance peak of about 40 nm, indicating that we can detach the PNA probe from the gold nanorod with vigorous sonication. To avoid this from happening, in all future experiments we used no more than 30 s of

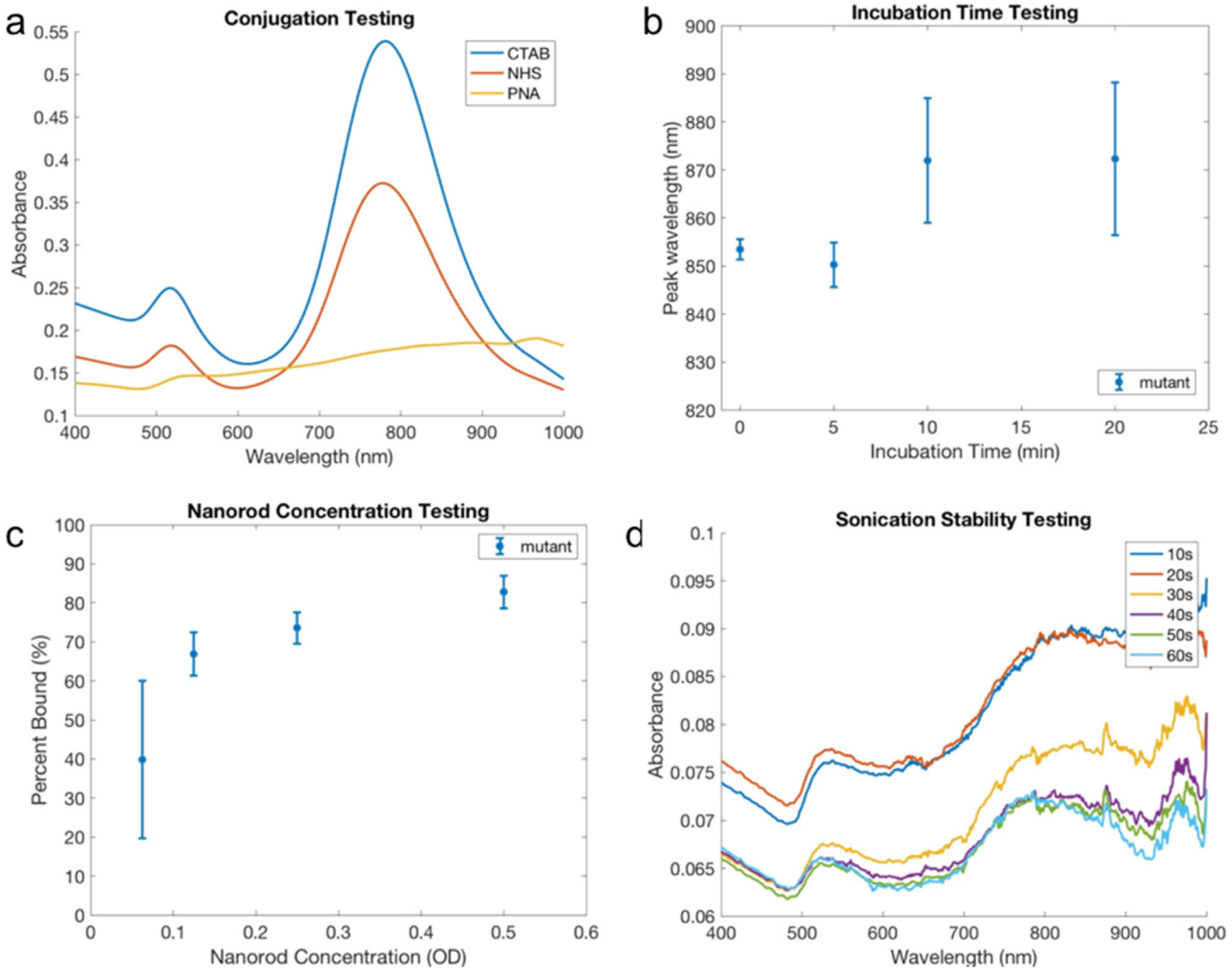

Fig. 3. (a) A demonstration of slight blue shift upon NHS activation, and then significant red shift and flattening after PNA conjugation (b) A demonstration showing that the sensor output reaches the expected output wavelength after about 10 min, indicating that 10 min is the correct incubation time (c) A demonstration of effects of nanorod concentration on percent DNA bound, showing that OD 0.25 is ideal for testing (d) Sonication stability testing showing that 30 s is the maximum sonication time based on the blue shift at 40 s and after indicating removal of the PNA probes.

sonication to disperse the nanorods for measurement.

From this series of experiments, we determined the optimal PNA conjugation protocol, and the ideal conditions for measurement of ctDNA binding to the sensor in both buffer and spiked healthy patient serum samples. The error bars in the figure represent the standard deviation of three samples, identifying the range of potential inter-sample variability. In subsequent experiments, a 10–15 min incubation time was used with a nanorod concentration of OD 0.25 and no more than 30 s of sonication for redispersion of the nanorods.

3.4. ctDNA sensing in buffer and spiked healthy patient samples

Using the optimized conjugation and binding conditions determined from the experiments described in the previous section, we tested the average peak wavelength of the sensors in response to a range of synthetic ctDNA. The clinically relevant metric from this test is whether the sensor binds mutant synthetic ctDNA at a higher rate than it binds the wild type synthetic ctDNA, because it is important to know the ratio of tumor-specific mutation present in the patient blood. For this study, we used the 15 bp PNA that is directly complimentary to the G12V mutant ctDNA and put the nanosensor in contact with both the exact complimentary 41 bp mutant ctDNA oligo and the 41 bp wild type oligo that has a single base pair mismatch. We tested nanorods at OD 0.25 and incubated them with each concentration of ctDNA for 15 min before measurement, centrifugation, and remaining ctDNA quantitation using the Qubit.

The data from these tests is shown in Fig. 4. In Fig. 4**a** we show four representative spectra at a range of synthetic ctDNA concentrations. The raw data and data with Lowess smoothing is plotted, along with the peak location calculated from the center of mass. This shows successive red shifts with increasing ctDNA concentration. We found that with increasing synthetic ctDNA concentration, we obtained linearly increasing sensor output with peak wavelength (Fig. 4**b**). We further found that the sensor bound more mutant DNA than wild type, indicating that the PNA probes showed some specificity for the exact complimentary sequence over the one with a single base pair mismatch. We also found, as shown in Fig. 4**c**, that the gold nanorods bound significantly more of the mutant ctDNA than the wild type sequence.

We then tested, using the same workflow, healthy patient serum samples spiked with known concentrations of ctDNA. This study provided insight into how the sensor would work in the clinic, and whether there would be any interference or nonspecific binding from other biomolecules in a serum sample. Another concern was that the nanorods and ctDNA would not achieve successful binding without an adequate salt concentration in the serum compared to TE buffer. We actually found that the sensor performance was unimpaired in serum samples, indicating that it can be easily translated to cancer patient samples for testing (Fig. 4**d**). One concern with this data is that there is

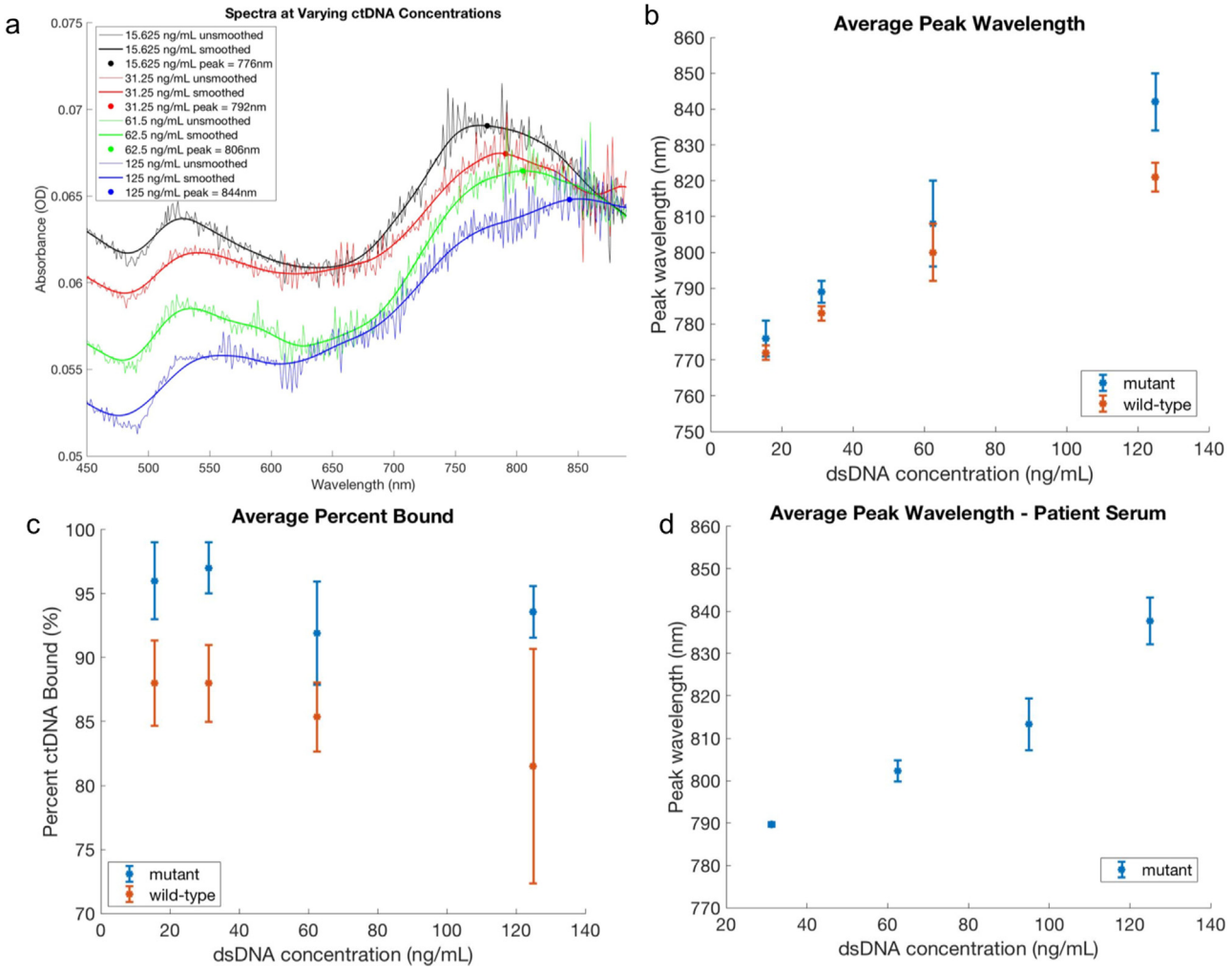

Fig. 4. Results of the synthetic ctDNA testing at a range of concentration. (a) Spectra for four concentrations of synthetic DNA in buffer. Raw data and data with Lowess smoothing overlaid in bold, and peaks marked and noted in the key (b) sensor output for three samples each of mutant and wild type ctDNA at three concentrations, demonstrating higher binding rate of mutant than wild type sequences, and a linear sensing working range (c) percentage of ctDNA binding rate, demonstrating that more of the mutant ctDNA was bound (d) sensor output for three samples of mutant ctDNA at four concentrations in spiked healthy patient serum.

not as much specificity, or discrimination between the mutant ctDNA and the wild type ctDNA as desired. We simulated the hybridization reactions to determine a way to design a PNA that improved upon the specificity of the exact complimentary sequence.

3.5. PNA-DNA hybridization simulations

In this section we sought to simulate the PNA-DNA binding to better design the PNA probe for specific capture of the G12V (c.35G > T) mutation versus the wild type. In all the trials run prior, the PNA used was exactly complimentary to the c.35G > T mutation, meaning that it had no mismatch with the mutant ctDNA, and one base pair mismatch with the wild type sequence. While this worked well for detecting synthetic ctDNA of increasing concentrations, the specificity for the point mutation of interest could be improved. This would manifest in the output as a larger gap between the mutant binding spectra peak and wild type binding spectra speak at the same concentrations. We were interested to see if the addition of mutations into the PNA (thereby giving 1 bp mismatch with the mutant and 2 bp mismatch with the wild type) would change the thermodynamics of the reaction enough to improve the selectivity.

Fig. 5 shows the results of this simulation in both numerical and graphical form. In panel Fig. 5**a**, each row represents a PNA with a different mutation and shows the melting temperature of each PNA with both the mutant and the wild type. The key candidates are those with the largest difference in melting temperature between the mutant and the wild type, indicating that the reaction is significantly more thermodynamically favoring binding with the mutant sequence. These are shown in color on the table and have additional mutations 2 base pairs removed from the c.35G > T mutation of interest.

This data is demonstrated in graphical form in Fig. 5**b**. The curves show two candidates which have a significantly high difference in melting temperature as the two higher points in the curve in Fig. 5**b**. These candidates are projected to have such a low binding affinity to the wild type sequence that they could improve selectivity to the mutant over the wild type. We also show the binding and mismatches in Fig. 5**c**, demonstrating where each of the mismatches is in relation to both the mutant and the wild type ctDNA sequence for the complimentary PNA and this new PNA with the additional mutation.

3.6. Improved PNA design hybridization testing

The simulation described in this section provided a new 15 bp PNA candidate that could improve selectivity of the sensor due to an added mutation that makes the thermodynamics of binding to the wild type sequence very unfavorable. We went through a similar process to the above steps and conjugated the gold nanorod with the new PNA candidate to determine if it improved the specificity of binding. We then

a

PNA Mutation	5' - PNA - 3'	Oligo	dH (kcal/mol)	dS (cal/mol/K)	dG (kcal/mol)	Tm (°C)	dTm (°C)
c.35G>T	TACGCCAACAGCTCC	wt	-105.6	-292.5	-18.4	42.5	4.7
		mut	-121.8	-338	-21	47.2	
c.35G>T, c.37G>T	TACGCAAACAGCTCC	wt	-96	-281	-12.2	24	12.5
		mut	-103	-290.5	-16.4	36.5	
c.35G>T, c.37G>A	TACGCTAACAGCTCC	wt	-92	-259.6	-14.6	31.8	6.6
		mut	-108.2	-305.2	-17.2	38.4	
c.35G>T, c.37G>C	TACGCGAACAGCTCC	wt	-95.9	-280.7	-12.2	24	13.8
		mut	-108.5	-306.8	-17	37.8	
c.35G>T, c.38G>T	TACGACAACAGCTCC	wt	-87.9	-246	-14.5	31.9	6.9
		mut	-104.1	-291.6	-17.2	38.8	
c.35G>T, c.38G>A	TACGTCAACAGCTCC	wt	-88.9	-250.1	-14.3	31.1	6.9
		mut	-105.1	-295.7	-16.9	38	
c.35G>T, c.38G>C	TACGGCAACAGCTCC	wt	-100.5	-282	-16.4	36.9	5.6
		mut	-116.7	-327.6	-19	42.5	
c.35G>T, c.32C>T	TACGCCAACAACTCC	wt	-86.4	-246.3	-13	26.5	7.6
		mut	-102.6	-291.8	-15.6	34.1	
c.35G>T, c.32C>A	TACGCCAACATCTCC	wt	-86.9	-247.9	-13	26.5	7.6
		mut	-103.1	-293.5	-15.6	34.1	
c.35G>T, c.32C>G	TACGCCAACACCTCC	wt	-84.5	-242.6	-12.2	23.6	8.1
		mut	-100.7	-288.2	-14.8	31.7	

b

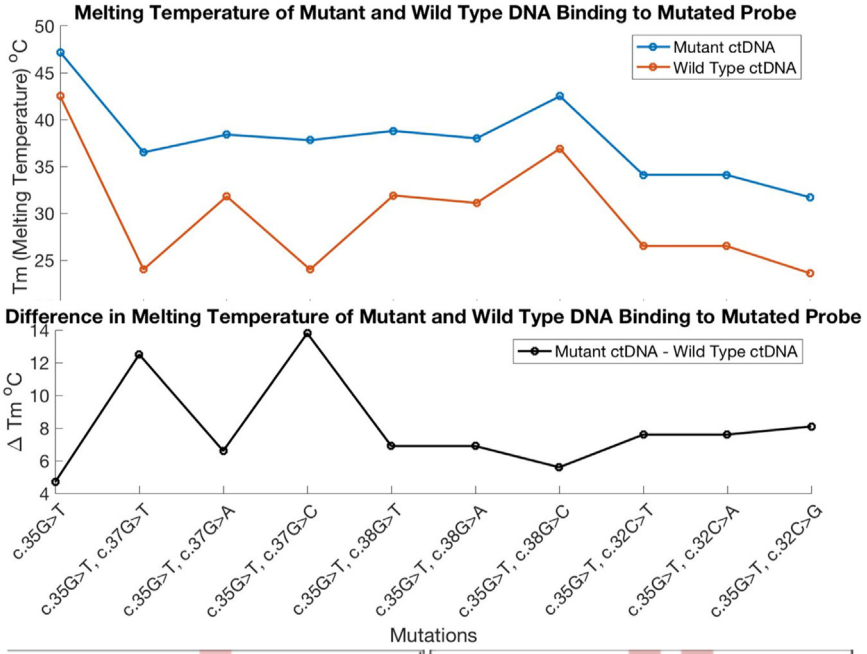

c

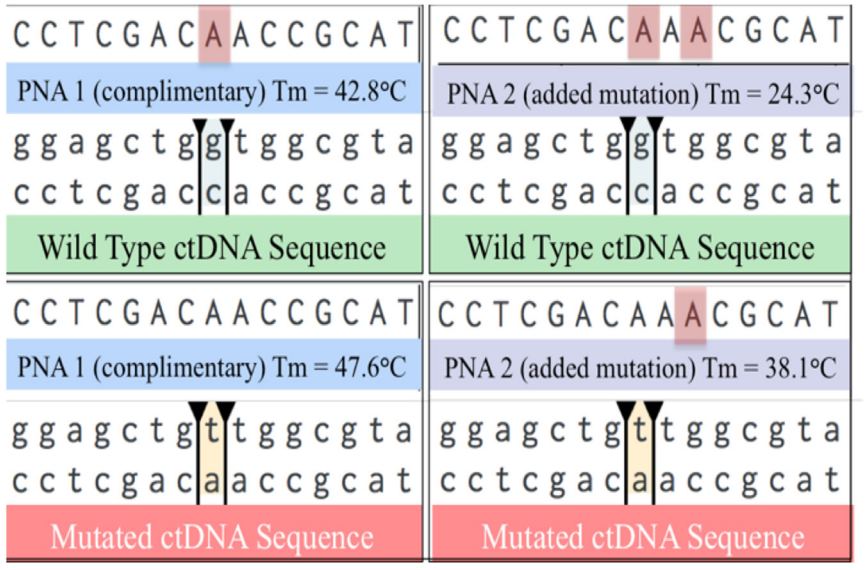

Fig. 5. Results of the Melting Temperature Simulation using DINAMelt. (a) Results of the Melting Temperature Simulation using DINAMelt. Each row represents a different PNA sequence with an added mutation. The first row shows the PNA complimentary to the G12V mutation. The two rows highlighted demonstrate the largest difference in binding affinity between the mutant and wild type sequences. (b) The melting temperature for both the mutant and wild type for each of the tested probes. Below is the difference of the melting temperatures, showing two mutations that are good candidates due to their large difference in melting temperature between the mutant and wild type (c) A visual representation of how the original PNA complimentary to the mutation and one of the new PNA candidates binds to both oligos, showing the additional mismatch on the wild type ctDNA oligo.

tested the binding of these new nanorods to three concentrations of mutant and wild type synthetic ctDNA in TE buffer using the same parameters as earlier. As shown in Fig. 6, we found a significant improvement in the selectivity of the sensor, which manifested as a larger gap between the sensing lines for the mutant and wild type samples. With the old complimentary PNA there was some overlap of

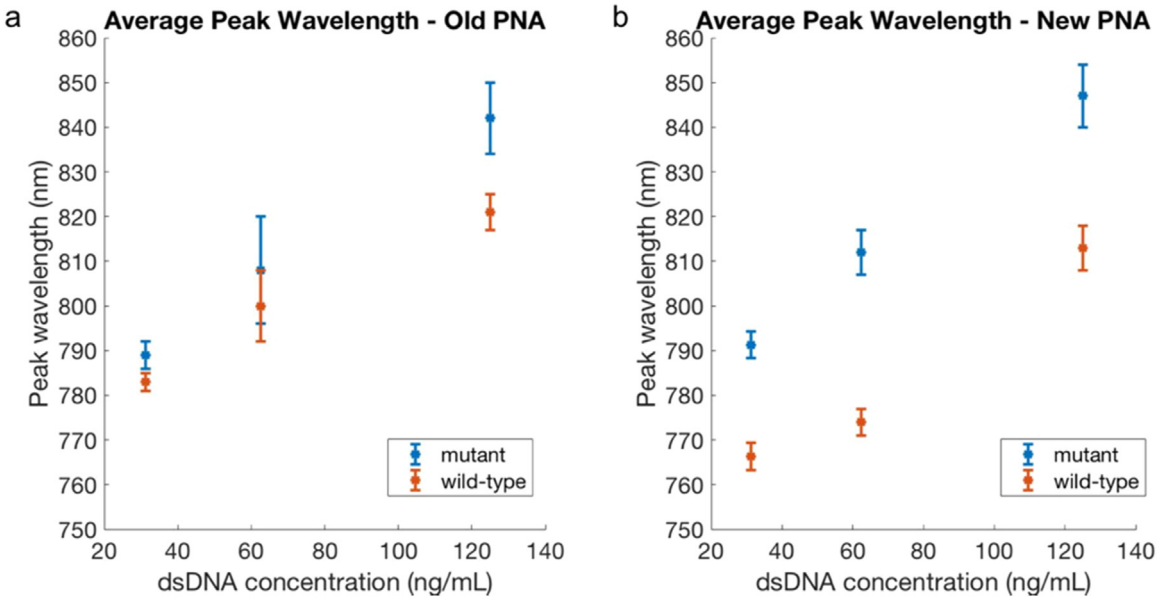

Fig. 6. Demonstration of the improvement from the new PNA sequence as a result of the simulation (a) The original PNA sensing data showing more binding to mutant but minimal separation between mutant and wild type sequence output (b) Significant separation between the mutant and wild type sequence output curves using the new PNA ($p < 0.01$).

signal as indicated by the error bars, particularly at a concentration of 62.5 ng/mL. With the new PNA there is a much clearer distinction between the linear sensing output for the mutant and the wild type sequences, and this difference is statistically significant ($p < 0.01$). This data is very promising because it shows the importance of probe design in affecting the thermodynamics of the capture reaction and eventually the selectivity of the device. This strategy could be very useful in future studies that are trying to elucidate allele variant frequency and differentiate point mutations from a background of wild type DNA molecules.

4. Conclusions

In this study, we demonstrate the development and optimization of a nanoplasmonic ctDNA for label-free detection of point mutations in the KRAS gene associated with pancreatic ductal adenocarcinoma. We are able to discriminate between the mutant and the wild-type sequence of the KRAS gene using gold nanorods in solution and were able to establish a detection range in the tens of nanograms per milliliter of buffer or patient serum. We demonstrated a linear working range for the device below 125 ng/mL ctDNA, and an effective limit of detection of 2 ng/mL in solution. We used a hybridization simulation method to improve the selectivity of PNA binding through the addition of another point mutation designed to make binding to the wild type ctDNA unfavorable. From the simulations, we selected a candidate with a large expected difference in binding affinity, and demonstrated a significant improvement in sensor selectivity with a $p < 0.01$.

The promising results presented here pave the way to achieve multiplexing and arrayed sensor designs. Current multiplexing approach to capture multiple sequences of ctDNA would involve multiple testing tubes but could be accomplished through integrating the principles described in this paper on-chip. In addition, the single sensor element can be scaled up to a sensor array, making smaller changes easily detectable at tunable spatial-temporal scale, to elucidate at extremely low biomarker concentration. Clinical validation could be designed to characterize a cohort of patient samples and healthy controls to validate the translational significance of the platform. The techniques demonstrated in this paper provide a strategy for sensitive and selective detection of a clinically relevant point mutation in the KRAS gene in both buffer and spiked patient serum.

CRediT authorship contribution statement

Amogha Tadimety: Conceptualization, Data curation, Formal analysis, Methodology, Writing - original draft, Writing - review & editing. **Yichen Zhang:** Data curation, Methodology, Validation, Writing - original draft, Writing - review & editing. **Kasia M. Kready:** Methodology, Validation, Writing - review & editing. **Timothy J. Palinski:** Formal analysis, Validation, Software, Writing - review & editing. **Gregory J. Tsongalis:** Resources, Validation, Writing - review & editing. **John X.J. Zhang:** Conceptualization, Funding acquisition, Investigation, Project administration, Validation, Resources, Writing - review & editing.

Acknowledgements

The authors are grateful for the financial support from the National Institutes of Health (NIH) Director's Transformative Research Award (United States) (R01HL137157), Norris Cotton Cancer Center Developmental Funds Pilot Projects (United States), and the Thayer School of Engineering PhD Innovation Program (United States). We would like to thank the undergraduates Cathy Li ‘19, George C. Cheng ‘19, and Morgan Lee ‘19 for their assistance on this project. We would also like to thank the DHMC Clinical Laboratories, especially Abigail Brunelle, for help with healthy patient samples. Finally, we would like to acknowledge Dr. Nanjing Hao for his help with electron microscopy for characterization.

Competing interests

The authors have no competing interests to declare.

Appendix A. Supporting information

Supplementary data associated with this article can be found in the online version at doi:10.1016/j.bios.2019.01.045.

References

Anker, P., Mulcahy, H., Chen, X.Q., Stroun, M., 1999. Detection of circulating tumour DNA in the blood (plasma/serum) of cancer patients. Cancer Metastas. Rev. 18, 65–73. https://doi.org/10.1023/A:1006260319913.

Bettegowda, C., Sausen, M., Leary, R.J., Kinde, I., Wang, Y., Agrawal, N., Bartlett, B.R., Wang, H., Luber, B., Alani, R.M., Antonarakis, E.S., Azad, N.S., Bardelli, A., Brem, H., Cameron, J.L., Lee, C.C., Fecher, L.A., Gallia, G.L., Gibbs, P., Le, D., Giuntoli, R.L., Goggins, M., Hogarty, M.D., Holdhoff, M., Hong, S.-M., Jiao, Y., Juhl, H.H., Kim, J.J., Siravegna, G., Laheru, D.A., Lauricella, C., Lim, M., Lipson, E.J., Marie, S.K.N., Netto, G.J., Oliner, K.S., Olivi, A., Olsson, L., Riggins, G.J., Sartore-Bianchi, A., Schmidt, K., Shih, L.-M., Oba-Shinjo, S.M., Siena, S., Theodorescu, D., Tie, J., Harkins, T.T., Veronese, S., Wang, T.-L., Weingart, J.D., Wolfgang, C.L., Wood, L.D., Xing, D., Hruban, R.H., Wu, J., Allen, P.J., Schmidt, C.M., Choti, M.A., Velculescu, V.E., Kinzler, K.W., Vogelstein, B., Papadopoulos, N., Diaz, L.A., 2014. Detection of circulating tumor DNA in early- and late-stage human malignancies. Sci. Transl. Med. 6, 1–11(https://doi.org/10.1126/scitranslmed.3007094).

Braun, G., Lee, S.J., Dante, M., Nguyen, T., Moskovits, M., Reich, N., 2007. Surface-Enhanced Raman Spectroscopy for DNA Detection by Nanoparticle Assembly onto Smooth Metal Films Surface-Enhanced Raman Spectroscopy for DNA Detection by Nanoparticle Assembly onto Smooth Metal Films, pp. 6378–6379. 〈https://doi.org/10.1021/ja070514z〉.

Brolo, A.G., 2012. Plasmonics for future biosensors. Nat. Photonics 6, 709–713. https://doi.org/10.1039/CT9232301986.

Chen, P., Huang, Y.-Y., Hoshino, K., Zhang, J.X.J., 2015. Microscale magnetic field modulation for enhanced capture and distribution of rare circulating tumor cells. Sci. Rep. 5, 8745. https://doi.org/10.1038/srep08745.

Dawson, S.-J., Tsui, D.W.Y., Murtaza, M., Biggs, H., Rueda, O.M., Chin, S.-F., Dunning, M.J., Gale, D., Forshew, T., Mahler-Araujo, B., Rajan, S., Humphray, S., Becq, J., Halsall, D., Wallis, M., Bentley, D., Caldas, C., Rosenfeld, N., 2013. Analysis of circulating tumor DNA to monitor metastatic breast cancer. N. Engl. J. Med. 368, 1199–1209. https://doi.org/10.1056/NEJMoa1213261.

Egatz-Gomez, A., Wang, C., Klacsmann, F., Pan, Z., Marczak, S., Wang, Y., Sun, G., Senapati, S., Chang, H.C., 2016. Future microfluidic and nanofluidic modular platforms for nucleic acid liquid biopsy in precision medicine. Biomicrofluidics 10. https://doi.org/10.1063/1.4948525.

Guo, L., Kim, D.H., 2012. LSPR biomolecular assay with high sensitivity induced by aptamer-antigen-antibody sandwich complex. Biosens. Bioelectron. 31, 567–570. https://doi.org/10.1016/j.bios.2011.10.047.

Hao, N., Zhang, J.X.J., 2017. Microfluidic screening of circulating tumor biomarkers toward liquid biopsy. Sep. Purif. Rev. 00, 1–30. https://doi.org/10.1080/15422119.2017.1320763.

Hoshino, K., Chung, H., Wu, C.-H., Rajendran, K., Huang, Y.-Y., Chen, P., Sokolov, K.V., Kim, J., Zhang, J.X.J., 2015. An immunofluorescence-assisted microfluidic single cell quantitative reverse transcription polymerase chain reaction analysis of tumour cells separated from blood. J. Circ. Biomark. 4, 1–5. https://doi.org/10.5772/61822.

Im, H., Bantz, K.C., Lee, S.H., Johnson, T.W., Haynes, C.L., Oh, S.H., 2013. Self-assembled plasmonic nanoring cavity arrays for SERS and LSPR biosensing. Adv. Mater. 25, 2678–2685. https://doi.org/10.1002/adma.201204283.

Jazayeri, M.H., Amani, H., Pourfatollah, A.A., Pazoki-Toroudi, H., Sedighimoghaddam, B., 2016. Various methods of gold nanoparticles (GNPs) conjugation to antibodies. Sens. Bio-Sens. Res. 9, 17–22. https://doi.org/10.1016/j.sbsr.2016.04.002.

Jia, S., Zhang, R., Li, Z., Li, J., 2015. Clinical and biological significance of circulating tumor cells, circulating tumor DNA, and exosomes as biomarkers in colorectal cancer. Oncotarget 9. https://doi.org/10.18632/oncotarget.17184.

Jiang, P., Lo, Y.M.D., 2016. The long and short of circulating cell-free DNA and the ins and outs of molecular diagnostics. Trends Genet. xx, 1–12. https://doi.org/10.1016/j.tig.2016.03.009.

Joshi, G.K., Deitz-mcelyea, S., Liyanage, T., Lawrence, K., 2015. Short Noncoding RNA Sensing at Attomolar Concentrations Allows for Quantitative and Highly Specific Assay of MicroRNA-10b in Biological Fluids and Circulating Exosomes. 〈https://doi.org/10.1021/acsnano.5b04527〉.

Kedem, O., Vaskevich, A., Rubinstein, I., 2011. Improved sensitivity of localized surface plasmon resonance transducers using reflection measurements. J. Phys. Chem. Lett. 2, 1223–1226. https://doi.org/10.1021/jz200482f.

Kinugasa, H., Nouso, K., Miyahara, K., Morimoto, Y., Dohi, C., Tsutsumi, K., Kato, H., Matsubara, T., Okada, H., Yamamoto, K., 2015. Detection of K-ras gene mutation by liquid biopsy in patients with pancreatic cancer. Cancer 121, 2271–2280. https://doi.org/10.1002/cncr.29364.

Lin, D.-Z., Chuang, P.-C., Liao, P.-C., Chen, J.-P., Chen, Y.-F., 2016. Increasing the spectral shifts in LSPR biosensing using DNA-functionalized gold nanorods in a competitive assay format for the detection of interferon-γ. Biosens. Bioelectron. 81, 221–228. https://doi.org/10.1016/j.bios.2016.02.071.

Lohse, J., Dahl, O., Nielsen, P.E., 1999. Double duplex invasion by peptide nucleic acid: a general principle for sequence-specific targeting of double-stranded DNA. Proc. Natl. Acad. Sci. USA 96, 11804–11808. https://doi.org/10.1073/pnas.96.21.11804.

López, S.O., García-Olmo, D.C., García-Arranz, M., Guadalajara, H., Pastor, C., García-Olmo, D., 2016. KRAS G12V mutation detection by droplet digital PCR in circulating cell-free DNA of colorectal cancer patients. Int. J. Mol. Sci. 17, 1–9. https://doi.org/10.3390/ijms17040484.

Ma, X., Truong, P.L., Anh, N.H., Sim, S.J., 2015. Single gold nanoplasmonic sensor for clinical cancer diagnosis based on specific interaction between nucleic acids and protein. Biosens. Bioelectron. 67, 59–65. https://doi.org/10.1016/j.bios.2014.06.038.

Mayer, K.M., Hafner, J.H., 2011. Localized surface plasmon resonance sensors. ACS Chem. Rev. 111, 3828–3857.

Ngernpimai, S., Matulakun, P., Teerasong, S., Puangmali, T., Kopwitthaya, A., Kanokmedhakul, S., Sangiamdee, D., Chompoosor, A., 2018. Gold nanorods enhanced resonance Rayleigh scattering for detection of Hg2+ by in-situ mixing with single-stranded DNA. Sens. Actuators B Chem. 255, 836–842. https://doi.org/10.1016/j.snb.2017.08.129.

Nguyen, A.H., Sim, S.J., 2015. Nanoplasmonic biosensor: detection and amplification of dual bio-signatures of circulating tumor DNA. Biosens. Bioelectron. 67, 443–449. https://doi.org/10.1016/j.bios.2014.09.003.

Ozkumur, E., Shah, A.M., Ciciliano, J.C., Emmink, B.L., Miyamoto, D.T., Brachtel, E., Yu, M., Chen, P.-I., Morgan, B., Trautwein, J., Kimura, A., Sengupta, S., Stott, S.L., Karabacak, N.M., Barber, T.A., Walsh, J.R., Smith, K., Spuhler, P.S., Sullivan, J.P., Lee, R.J., Ting, D.T., Luo, X., Shaw, A.T., Bardia, A., Sequist, L.V., Louis, D.N., Maheswaran, S., Kapur, R., Haber, D.A., Toner, M., 2013. Inertial focusing for tumor antigen-dependent and -independent sorting of rare circulating tumor cells. Sci. Transl. Med. 5. https://doi.org/10.1126/scitranslmed.3005616.

Ray, A., Nordén, B., 2000. Peptide nucleic acid (PNA): its medical and biotechnical applications and promise for the future. FASEB J. 14, 1041–1060 (https://doi.org/14(9)1041-1060).

Sausen, M., Phallen, J., Adleff, V., Jones, S., Leary, R.J., Barrett, M.T., Anagnostou, V., Parpart-Li, S., Murphy, D., Li, Q.K., Hruban, C.A., Scharpf, R., White, J.R., O'Dwyer, P.J., Allen, P.J., Eshleman, J.R., Thompson, C.B., Klimstra, D.S., Linehan, D.C., Maitra, A., Hruban, R.H., Diaz, L.A., Von Hoff, D.D., Johansen, J.S., Drebin, J.A., Velculescu, V.E., 2015. Clinical implications of genomic alterations in the tumour and circulation of pancreatic cancer patients. Nat. Commun. 6, 1–6. https://doi.org/10.1038/ncomms8686.

Sepúlveda, B., Angelomé, P.C., Lechuga, L.M., Liz-Marzán, L.M., 2009. LSPR-based nanobiosensors. Nano Today 4, 244–251. https://doi.org/10.1016/j.nantod.2009.04.001.

Siddiquee, S., Rovin, K., Azriah, A., 2015. A review of peptide nucleic acid. Adv. Tech. Biol. Med. 3, 1–10. https://doi.org/10.4172/2379-1764.

Siegel, R.L., Miller, K.D., Jemal, A., 2018. Cancer statistics, 2018. Ca. Cancer J. Clin. 67, 7–30. https://doi.org/10.3322/caac.21387.

Tadimety, A., Closson, A., Li, C., Yi, S., Shen, T., Zhang, J.X.J., 2018. Advances in liquid biopsy on-chip for cancer management: technologies, biomarkers, and clinical analysis. Crit. Rev. Clin. Lab. Sci. 1–23. https://doi.org/10.1080/10408363.2018.1425976.

Tadimety, A., Syed, A., Nie, Y., Long, C.R., Kready, K.M., Zhang, J.X.J., 2017a. Liquid biopsy on chip: a paradigm shift towards the understanding of cancer metastasis. Integr. Biol. 64, 9–29. https://doi.org/10.1039/C6IB00202A.

Tadimety, A., Zhang, Y., Tsongalis, G.J., Z.J.X.J, 2017b. Screening circulating nucleic acids of pancreatic ductal adenocarcinoma using a plasmonic nanosensor. J. Mol. Diagn. 915. https://doi.org/10.1016/S1525-1578(15)00191-9.

Taylor, A.B., Zijlstra, P., 2017. Single-molecule plasmon sensing: current status and future prospects. ACS Sens. 2, 1103–1122. https://doi.org/10.1021/acssensors.7b00382.

Wang, S., Sato, S., Kimura, K., 2003. Preparation of hexagonal-close-packed colloidal crystals of hydrophilic monodisperse gold nanoparticles in bulk aqueous solution. Chem. Mater. 15, 2445–2448. https://doi.org/10.1021/cm0217147.

Wang, S., Sim, W.S., 2006. Au nanoparticles encapsulated in Ru carbonyl carboxylate shells. Langmuir 22, 7861–7866. https://doi.org/10.1021/la060784f.

Zhang, N., Appella, D.H., 2010. Advantages of peptide nucleic acids as diagnostic platforms for detection of nucleic acids in resource-limited settings. J. Infect. Dis. 201, S42–S45. https://doi.org/10.1086/650389.

Zhang, W., Xia, W., Lv, Z., Ni, C., Xin, Y., Yang, L., 2017. Liquid biopsy for cancer: circulating tumor cells, circulating free DNA or exosomes? Cell. Physiol. Biochem. 755–768. https://doi.org/10.1159/000458736.